# Mesostructured Metal Germanium Sulfides

**Mark J. MacLachlan,[†] Neil Coombs,[†] Robert L. Bedard,[‡] Steve White,[§] Laurence K. Thompson,[§] and Geoffrey A. Ozin*[,†]**

*Contribution from the Materials Chemistry Research Group, Department of Chemistry, University of Toronto, 80 St. George Street, Toronto, Ontario, M5S 3H6, Canada; UOP, 50 East Algonquin Road, Des Plaines, Illinois 60017-5017; and the Department of Chemistry, Memorial University, St. John's, Newfoundland, A1B 3X7, Canada*

*Received July 27, 1999*

**Abstract:** A new class of mesostructured metal germanium sulfide materials has been prepared and characterized. The synthesis, via supramolecular assembly of well-defined germanium sulfide anionic cluster precursors and transition-metal cations in formamide, represents a new strategy for the formation of this class of solids. A variety of techniques were employed to examine the structure and composition of the materials. Structurally, the material is best described as a periodic mesostructured metal sulfide-based coordination framework akin to periodic hexagonal mesoporous silica, MCM-41. At the molecular scale, the materials strongly resemble microstructured metal germanium sulfides, in which the structure of the $[Ge_4S_{10}]^{4-}$ cluster building-blocks are intact and linked via $\mu$-S−M−S bonds. Evidence for a metal−metal bond in mesostructured $Cu/Ge_4S_{10}$ is also provided.

## Introduction

Microporous (pore diameters < 20 Å) and mesoporous (pore diameters 20−500 Å) materials (IUPAC convention[1]) are used extensively as heterogeneous catalysts, adsorption media, and ion-exchange materials.[2] For example, zeolites possess a crystalline microporosity, a very narrow pore size distribution, and a large surface area. These properties make them ideal for such diverse applications as water-softening, radioisotope removal from sites of nuclear contamination, and xylenes isomerization catalysis.[3] The discovery of aluminophosphate molecular sieves by Flanigen et al. initiated the exploration of the periodic table for novel microporous materials.[4] Since then, microporous materials have incorporated a variety of transition- and main-group elements.[5]

In 1989, Bedard et al. patented a new class of microporous metal germanium sulfides (denoted GS-3 for its structure type) prepared hydrothermally from the elements.[6,7] Yaghi et al. subsequently showed that these materials could be prepared at room temperature.[8] When adamantanoid $[Ge_4S_{10}]^{4-}$ clusters were combined with manganese acetate in water, crystals of the microporous manganese germanium sulfide formed. The framework contains tetradentate $[Ge_4S_{10}]^{4-}$ clusters linked with transition metals to form a zinc blende framework of $Mn^{2+}/[Ge_4S_{10}]^{4-}$ with the charge balancing TMA (tetramethylammonium) cations included in the pores. Others and we have extended this class of materials to incorporate a variety of templates and metals, including $[Ag_2]^{2+}$ and $[Cu_2]^{2+}$ dimers when silver or copper salts are introduced into the preparation.[9−11]

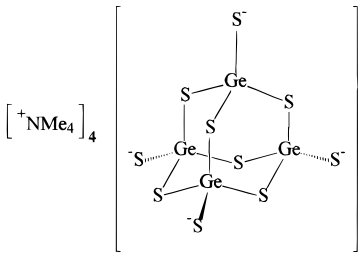


The discovery of liquid-crystal templating of silica in 1992 represented a breakthrough in inorganic materials chemistry.[12,13]

[†] University of Toronto.
[‡] UOP.
[§] Memorial University.

(1) IUPAC Manual of Symbols and Terminology, Appendix 2, Part 1, Colloid and Surface Science. *Pure Appl. Chem.* **1972**, *31*, 578.

(2) For example, see: (a) Szostak, R. *Molecular Sieves: Principles of Synthesis and Identification*; Van Nostrand Rheinhold: New York, 1989. (b) Moser, W. R. *Advanced Catalysis and Nanostructured Materials: Modern Synthetic Methods*; Academic Press: London, 1996. (c) Breck, D. W. *Zeolite Molecular Sieves*; John Wiley: New York, 1974.

(3) Smart, L.; Moore, E. *Solid State Chemistry, An Introduction*, 2nd ed.; Chapman & Hill: New York, 1995.

(4) (a) Wilson, S. T.; Lok, B. M.; Messina, C. A.; Cannan, T. R.; Flanigen, E. M. *J. Am. Chem. Soc.* **1982**, *104*, 1146. (b) Wilson, S. T.; Lok, B. M.; Flanigen, E. M. U.S. Patent 4,320,440; 1982.

(5) Bowes, C. L.; Ozin, G. A. *Adv. Mater.* **1996**, *8*, 13.

(6) Bedard, R. L.; Vail, L. D.; Wilson, S. T.; Flanigen, E. M. U.S. Patent 4,933,068; 1990.

(7) Bedard, R. L.; Wilson, S. T.; Vail, L. D.; Bennett, J. M.; Flanigen, E. M. In *Zeolites: Facts, Figures, Future;* Jacobs, P. A., van Santen, R. A., Eds.; Elsevier: Amsterdam, 1989; p 375.

(8) Yaghi, O. M.; Sun, Z.; Richardson, D. A.; Groy, T. L. *J. Am. Chem. Soc.* **1994**, *116*, 807.

(9) (a) Bowes, C. L.; Lough, A. J.; Malek, A.; Ozin, G. A.; Petrov, S.; Young, D. *Chem. Ber.* **1996**, *129*, 283. (b) Yaghi, O. M.; Richardson, D. A.; Li, G.; Davis, C. E.; Groy, T. L. *Mater. Res. Symp. Proc.* **1995**, *371*, 15.

(10) Metal-linked $[Ge_4S_{10}]^{4-}$ and $[Ge_4Se_{10}]^{4-}$ clusters have been incorporated into materials hydrothermally by several researchers. For example, see: (a) Cahill, C. L.; Parise, J. B. *Chem. Mater.* **1997**, *9*, 807. (b) Parise, J. B.; Tan, K. *Chem. Commun.* **1996**, 1687. (c) Loose, A.; Sheldrick, W. S. *Z. Naturforsch.* **1997**, 687. (d) Achak, O.; Pivan, J. Y.; Maunaye, M.; Louër, M.; Louër, D. *J. Alloys Compd.* **1995**, *219*, 111. (e) Achak, O.; Pivan, J. Y.; Maunaye, M.; Louër, M.; Louër, D. *J. Solid State Chem.* **1996**, *121*, 473.

(11) Bowes, C. L.; Huynh, W. U.; Kirkby, S. J.; Malek, A.; Ozin, G. A.; Petrov, S.; Twardowski, M.; Young, D.; Bedard, R. L.; Broach, R. *Chem. Mater.* **1996**, *8*, 2147.

(12) Kresge, C. T.; Leonowicz, M. E.; Roth, W. J.; Vartuli, J. C.; Beck, J. S. *Nature* **1992**, *359*, 710.

10.1021/ja992663q CCC: $18.00 
Published on Web 12/04/1999

A periodic hexagonal honeycomb of silica was prepared by sol−gel condensation of silicates templated by the lyotropic liquid crystalline phase of a surfactant. Although the material is amorphous at the microscale, it has crystalline mesoporosity with well-ordered and aligned surfactant-filled silica channels. The surfactant can be removed from the material by calcination, solvent extraction, or even supercritical $CO_2$ extraction.[14] By varying the length of the surfactant, pore size can be controlled to angstrom precision. Hydrophobic molecules serve to swell the liquid crystalline phase and have been used to prepare materials with 20−100 Å pore diameters.

Mesostructured materials are generally prepared by trial-and-error using poorly defined precursors that assemble via condensation. Although the materials possess long-range order at the mesoscale, short-range order is not generally observed. There have been a few attempts to link cluster building blocks (e.g., Keggin ions[15]) into a mesoporous material, but they have been unsuccessful.

To date, nearly all well-characterized, hexagonally mesostructured materials have been based on oxides. Mesostructured sulfides have been sought after because of their anticipated electronic and optical properties and their affinity for heavy metals. There have been some reports of mesostructured sulfides, but most of these materials were poorly characterized. The synthesis of mesostructured sulfide-based materials has been hindered by the absence of suitable precursors and the poorly understood condensation behavior of metal sulfides. Stupp et al. reported that hexagonally organized CdS, CdSe, and ZnS could be formed by flowing $H_2S$ or $H_2Se$ over a hexagonal mesophase containing oligoethylene oxide oleyl ether ($C_{18}H_{35}(OCH_2CH_2)_{10}OH$), water, and a Cd(II) salt.[16] Ozin and coworkers have reported a liquid crystalline, mesostructured tin sulfide.[17]

Kanatzidis et al. reported the synthesis and structural characterization of lamellar assemblies of $[Ge_4S_{10}]^{4-}$ clusters charge-balanced by surfactants.[18] In these structures, the clusters formed hexagonal close-packed lamellae with interdigitated surfactant molecules between the layers. The clusters in this material were not connected. The same group has very recently reported the hydrothermal synthesis of a hexagonal mesostructured Mn/$Ge_4S_{10}$ material with mesityltrimethylammonium bromide as the surfactant.[18b] Prior to this, we reported that a well-ordered mesostructured metal germanium sulfide framework could be assembled from $TMA_4Ge_4S_{10}$, transition-metal salts, and surfactants in formamide.[19] Here, we report further information on the synthesis and characterization of mesostructured metal germanium sulfides.

## Experimental Section

**Materials.** $TMA_4Ge_4S_{10}$ was prepared hydrothermally by the literature method.[9a] $Ni(NO_3)_2{\cdot}6H_2O$ and tetradecyltrimethylammonium bromide (TDTBr) were obtained from BDH and Fluka, respectively. $CoSO_4{\cdot}7H_2O$ and CuCl were obtained from Fisher Scientific. Cetyltrimethylammonium bromide (CTABr), cetylpyridinium chloride monohydrate (CPMCl), octadecyltrimethylammonium bromide (ODTBr), $ZnCl_2$, dodecyltrimethylammonium bromide, and formamide (98%) were purchased from Aldrich. All reagents were used without further purification.

**Equipment.** All reactions were carried out in 20 mL capped vials under air. Solid-state 400 MHz $^1$H MAS (magic-angle spinning) and 100.5 MHz $^{13}$C CP (cross-polarization)-MAS NMR spectra were obtained on a Bruker DSX 400 spectrometer. Powder X-ray diffraction (PXRD) patterns were obtained on a Siemens D5000 X-ray diffractometer using Ni-filtered Cu Kα radiation ($\lambda = 1.541\,78$ Å). In diffraction patterns where the (110) and (200) reflections could not be resolved, peaks were fit using a Voigt function. Fits were generally in excellent agreement with the values predicted from the $d_{100}$ value. Variable-temperature PXRD patterns were obtained on the same instrument. The sample was layered onto a thin platinum strip in a hexanes suspension. Under vacuum, the sample was heated at ca. 5 °C min$^{-1}$ between data collection temperatures (100, 150, and 200 °C and every 20 °C after that) where it was held for ca. 10 min for data collection. Reflectance UV−vis/near-IR spectra were obtained on a Perkin-Elmer Lambda 900 UV−vis/near-IR spectrometer. Following Kubelka−Munk transformation, the data were fit to Gaussian line shapes to estimate the number of contributing peaks. IR spectra were obtained using KBr pellets on a Perkin-Elmer Paragon 500 FT-IR spectrometer. FT-Raman spectra were collected on a Bomems MB-157 FT-spectrometer with a Spectra Physics diode pumped Nd:YLF laser (1064 nm; 350 kHz repetition rate). The instrument was configured in 180° backscattering mode using sealed glass capillary tubes to hold the neat, crystalline samples. Pyrolysis mass spectra were obtained using a VG 70−250S mass spectrometer. Samples were heated at 32 °C min$^{-1}$, and the volatile products were ionized by EI. Thermogravimetric analyses were obtained on a Perkin-Elmer TGA-7 analyzer equipped with a TAC-7 instrument controller. Samples were heated at a rate of 5 °C min$^{-1}$ under a flow of $N_2$. Transmission electron micrographs were obtained with a Phillips 430 microscope operating at 100 kV. Whole mounted samples were placed directly on a carbon grid as the embedding media used for sectioning the samples reacted with the materials. Room temperature magnetic susceptibilities were measured by the Faraday method using a Cahn 7600 Faraday magnetic balance. Elemental analyses were performed at UOP, Des Plaines, IL. For sulfur analyses, samples were combusted in a tube furnace, and the $SO_2$ was analyzed by IR (relative error 5%). C, N, and H analyses were done by the standard combustion method (relative error 3−4%). Ge, Co, Cu, Zn, Cl, and Br analyses were performed by ICP (inductively coupled plasma) after dissolution or fusion with a flux (variable sample pretreatment, depending on solubility) (relative error 2%). To determine water content, samples were heated in a tube furnace, and the steam was dissolved in a solvent. The moisture content was then determined by a Karl Fischer titration.

**Synthesis.** Many samples of the mesostructured metal germanium sulfides were prepared with different metals (Co, Cu, Zn, Ni), surfactants ($C_nH_{2n+1}NMe_3^+X^-$ [$n$ = 12, 14, 16, 18; X = $Br^-$, $Cl^-$], $C_{16}H_{33}(NC_5H_5)^+Cl^-$), concentrations, and aging times (0−7 d). Examples of typical preparations are listed below along with the particular data measured for that sample. The materials are designated SURF−M/$Ge_4S_{10}$, where SURF = surfactant (CTA = cetyltrimethylammonium, CPM = cetylpyridinium, and TDT = tetradecyltrimethylammonium) and M indicates the metal used. In each synthesis it was necessary to first heat the surfactant−cluster assembly to 100−120 °C to solubilize the precursors and then to cool the solution to 80 °C for the reaction.

**CTA−Ni/$Ge_4S_{10}$.** A solution of 642 mg $Ni(NO_3)_2{\cdot}6H_2O$ (2.21 mmol) in 2 mL of formamide at 80 °C was added with a pipet to a solution of 1.00 g (1.10 mmol) of $TMA_4Ge_4S_{10}$, 1.50 g (4.12 mmol) of CTABr, and 14 mL of formamide at 80 °C. A brown precipitate immediately formed from the clear, colorless solution. The contents were shaken for ca. 5 s and then aged at 80 °C for 16 h. The product was isolated on a Buchner funnel, washed with formamide at 80 °C (ca. 50 mL), and then water at 80 °C (ca. 50 mL). The brown solid was dried under ambient conditions for 24 h prior to characterization. Yield: 1.37 g.

**Data for CTA−Ni/$Ge_4S_{10}$.** PXRD: 34.2 ($d_{100}$), 19.7 ($d_{110}$), 17.2 ($d_{200}$), 13.0 ($d_{210}$) Å. UV−vis/near-IR: $\lambda_{max}$ = 2458w, 2417w, 2365w,

(13) Beck, J. S.; Vartuli, J. C.; Roth, W. J.; Leonowicz, M. E.; Kresge, C. T.; Schmitt, K. D.; Chu, C. T.-W.; Olson, D. H.; Sheppard, E. W.; McCullen, S. B.; Higgins, J. B.; Schlenker, J. L. *J. Am. Chem. Soc.* **1992**, *114*, 10834.

(14) Kawi, S.; Lai, M. W. *Chem. Commun.* **1998**, 1407.

(15) Stein, A.; Fendorf, M.; Jarvie, T. P.; Mueller, K. T.; Benesi, A. J.; Mallouk, T. E. *Chem. Mater.* **1995**, *7*, 304.

(16) (a) Braun, P. V.; Osenar, P.; Stupp, S. I. *Nature* **1996**, *380*, 325. (b) Tohver, V.; Braun, P. V.; Pralle, M. U.; Stupp, S. I. *Chem. Mater.* **1997**, *9*, 1495. (c) Braun, P. V.; Osenar, P.; Tohver, V.; Kennedy, S. B.; Stupp, S. I. *J. Am. Chem. Soc.* **1999**, *121*, 7302.

(17) Jiang, T.; Ozin, G. A. *J. Mater. Chem.* **1997**, *7*, 2213.

(18) (a) Bonhomme, F.; Kanatzidis, M. G. *Chem. Mater.* **1998**, *10*, 1153. (b) Rangan, K. K.; Billinge, S. J. L.; Petkov, V.; Heising, J.; Kanatzidis, M. G. *Chem. Mater.* **1999**, *11*, in press.

(19) MacLachlan, M. J.; Coombs, N.; Ozin, G. A. *Nature* **1999**, *397*, 681.

2327w, 2270w, 1956m, 1778w, 1747w, 1681w, 379s. Anal. Found (%): Ni, 6.12; Ge, 20.5; S, 19; C, 35.6; N, 2.1; H, 6.9. Ash (500 °C): 52%.

**CTA−Cu/$Ge_4S_{10}$.** A mixture of 437 mg of CuCl in 4 mL of formamide at 80 °C was filtered, leaving ca. 300 mg (3 mmol) of CuCl in solution. This was added quickly with a pipet to a solution of 1.00 g (1.10 mmol) of $TMA_4Ge_4S_{10}$, 1.50 g of (4.12 mmol) CTABr, and 14 mL of formamide at 80 °C. A brown-yellow precipitate immediately formed. The mixture was shaken for ca. 5 s and then placed in an oven at 80 °C for 18 h. The product was isolated on a Buchner funnel and washed with formamide at 80 °C (ca. 50 mL) and water at 80 °C (ca. 50 mL). The powder was dried under ambient conditions for 24 h prior to characterization. Yield: 1.43 g of yellow-green powder.

**Data for CTA−Cu/$Ge_4S_{10}$.** PXRD: $d$ = 34.2 ($d_{100}$), 19.8 ($d_{110}$), 17.4 ($d_{200}$) Å. UV−vis/near-IR: $\lambda_{max}$ = 2369w, 1941w, 362s nm. Anal. Found (%): Cu, 14.9; Ge, 18.2; S, 20; C, 32.4; N, 1.8; H, 6.1. Ash (500 °C): 56%.

**CTA−Co/$Ge_4S_{10}$.** A solution of 87 mg (0.31 mmol) of $CoSO_4 \cdot 7H_2O$ in 1 g of formamide at 80 °C was added quickly with a pipet to a solution of 0.189 g (0.208 mmol) of $TMA_4Ge_4S_{10}$, 0.205 g of (0.562 mmol) CTABr, and 2.08 g of formamide at 80 °C. A blue precipitate formed immediately. The mixture was shaken for ca. 5 s and then filtered onto a Buchner funnel. The product was washed with formamide at 80 °C (ca. 20 mL) and then water at 80 °C (ca. 20 mL). The aqueous wash resulted in a color change of the powder from blue to green. After drying under ambient conditions for 24 h, the product was characterized. Yield: 0.13 g of green powder.

**Data for CTA−Co/$Ge_4S_{10}$.** PXRD: $d$ = 36.0 ($d_{100}$), 20.4 ($d_{110}$), 18.0 ($d_{200}$) Å. UV−vis/near-IR: $\lambda_{max}$ = 2414w, 2365w, 2329w, 2270w, 1600s (very broad), 720s, 362s. Anal. Found (%): Co, 4.49; Ge, 20.2; S, 23; C, 39.2; N, 2.2; H, 8.1.

**CTA−Zn/$Ge_4S_{10}$.** A solution of 305 mg $ZnCl_2$ (2.24 mmol) in 2 mL of formamide at 80 °C was added quickly with a pipet to a solution of 1.00 g (1.10 mmol) of $TMA_4Ge_4S_{10}$, 1.50 g (4.12 mmol) of CTABr, and 14 mL of formamide at 80 °C. A white precipitate formed immediately. The mixture was shaken for ca. 5 s and then aged at 80 °C for 9 h. The white product was isolated on a Buchner funnel and washed with ca. 50 mL of formamide (80 °C) and then ca. 50 mL of distilled water (80 °C). After drying overnight under ambient conditions, the product was characterized. Yield: 1.41 g of white powder.

**Data for CTA−Zn/$Ge_4S_{10}$.** PXRD: 33.7 ($d_{100}$), 19.2 ($d_{110}$), 16.8 ($d_{200}$) Å. UV−vis/near-IR: $\lambda_{max}$ = 2423w, 2367w, 2327w, 2274w, 1956w, 1778w, 1746w, 1689w, 1432w, 1231w, 301s nm. Anal. Found (%): Zn, 8.87; Ge, 20.6; S, 19; C, 36.0; N, 2.1; H, 7.3; Cl, 0.023; Br, <0.01; $H_2O$, 8.06. Ash (500 °C): 53%.

**CPM−Zn/$Ge_4S_{10}$.** A solution containing 320 mg of $ZnCl_2$ (2.35 mmol) in 2 mL of formamide at 80 °C was added quickly with a pipet to a solution of 1.00 g (1.10 mmol) of $TMA_4Ge_4S_{10}$, 1.00 g (2.79 mmol) of $CPMCl \cdot H_2O$, and 14 mL of formamide at 80 °C. A white precipitate formed immediately. The mixture was shaken briefly (ca. 5 s) and then aged for 18 h at 80 °C. The product was isolated on a Buchner funnel, washed with ca. 50 mL of formamide (80 °C) and then ca. 50 mL of water (80 °C), and dried overnight under ambient conditions. Yield: 1.30 g of white powder.

**Data for CPM−Zn/$Ge_4S_{10}$.** PXRD: $d$ = 34.5 ($d_{100}$), 19.5 ($d_{110}$), 17.2 ($d_{200}$) Å. UV−vis/near-IR: $\lambda_{max}$ = 2438w, 2367w, 2327w, 2155w, 1957w, 1779w, 1746w, 1677w, 1433w, 1409w, 1231w, 311s. Anal. Found (%): Zn, 7.8; Ge, 22.4; S, 22; C, 35.4; N, 1.9; H, 6.0; Cl, 0.21; Br, <0.01; $H_2O$, 3.51. Ash (500 °C): 50%.

**TDT-Ni/$Ge_4S_{10}$.** A solution of 255 mg of $Ni(NO_3)_2 \cdot 6H_2O$ in 2 mL of formamide at 80 °C was added quickly with a pipet to a solution of 643 mg (0.708 mmol) of $TMA_4Ge_4S_{10}$, 1.00 g of (2.97 mmol) tetradecyltrimethylammonium bromide (TDTBr), and 10 mL of formamide. A brown precipitate immediately formed. After the mixture was shaken for ca. 5 s, it was aged at 80 °C for 20 h. The product was isolated on a Buchner funnel and washed with ca. 50 mL of formamide (80 °C) and then ca. 50 mL of water (80 °C). A fine brown powder was obtained after drying overnight under ambient conditions. Yield: 596 mg.

**Data for TDT−Ni/$Ge_4S_{10}$.** PXRD: $d$ = 31.6 ($d_{100}$), 18.0 ($d_{110}$), 15.8 ($d_{200}$) Å. UV−vis/near-IR: $\lambda_{max}$ = 2419w, 2367w, 2331w, 2269w, 1971m, 1781w, 1747w, 1687w, 366s nm. Anal. Found (%): Ni, 6.8; Ge, 21.3; S, 22; C, 33.3; N, 1.9; H, 6.6. Ash (500 °C): 41%.

**Table 1.** Summary of Elemental Analysis Results for Mesostructured Metal Germanium Sulfides

| sample | S:$Ge_4$ found | N:$Ge_4$ found | M:$Ge_4$ found | M:$Ge_4$ used |
|---|---|---|---|---|
| Zn[a] | 9.9(5)[a] | 2.26 | 2.12 | 2.0 |
| Zn[a] | 8.4(4)[a] | 2.11 | 1.91 | 2.1 |
| Zn[b] | 9.0(5)[b] | 1.76 | 1.55 | 2.1 |
| Cu[a] | 9.9(5)[a] | 2.05 | 3.74 | 2.7 |
| Co[a] | 10.3(5)[c] | 2.26 | 1.10 | 1.5 |
| Co[a] | 11.6(6)[c] | 2.07 | 1.94 | 2.3 |
| Ni[d] | 9.7(5) | 2.22 | 1.42 | 1.2 |
| Ni[a] | 10.5(5) | 2.14 | 2.57 | 1.9 |
| Ni[a] | 8.2(4) | 2.12 | 1.48 | 2.0 |
| Ni[e] | 9.3(5) | 1.85 | 1.58 | 1.2 |

[a] Prepared with CTABr as template. [b] Prepared with CPMCl as template. [c] Cobalt sulfate was the metal source and may explain why the S analyses are high. [d] Prepared with $C_{12}H_{25}NMe_3^+Cl^-$ as template. [e] Prepared with TDTBr as template.

## Results

**Synthesis.** We identified the linking of $[Ge_4S_{10}]^{4-}$ clusters with transition metals as a route to a new type of mesostructured material. Initially, a series of $[Ge_4S_{10}]^{4-}$ clusters charge-balanced with surfactants ($[C_nH_{2n+1}NMe_3]_4Ge_4S_{10}$, $n$ = 12, 14, 16, 18) was prepared to serve as precursors for the mesostructured materials. They were found to have low solubility in common solvents that form lyotropic liquid crystalline phases (e.g., water, ethanol, ethylene glycol) but were very soluble in warm (ca. 80 °C) formamide. A preliminary reaction of $(C_{12}H_{25}NMe_3)_4Ge_4S_{10}$ with $ZnCl_2$ in formamide gave a material that showed a peak in the PXRD pattern, $d_{100}$ = 37 Å. We felt that a synthesis directly from $TMA_4Ge_4S_{10}$ would be a more convenient route.

In a typical preparation, $TMA_4Ge_4S_{10}$ and the surfactant were dissolved in formamide to form a clear, viscous liquid. Rapid addition of $CoSO_4$, $Ni(NO_3)_2$, $ZnCl_2$, or CuCl in formamide at 80 °C immediately gave a precipitate. After being aged at 80 °C, the products were isolated, washed with hot formamide and then water, and dried under ambient conditions. The products were all light, free-flowing powders obtained in reasonable yields. A variety of cationic surfactant templates were used. PXRD patterns of the materials indicated that they all possessed hexagonal symmetry; evidence for a lamellar phase was only observed in samples prepared with $C_{18}H_{37}NMe_3^+$ as surfactant.

Ge, S, Cl, Br, C, N, H, $H_2O$, and metal analyses were obtained for several samples of the mesostructured materials. A summary of the data is provided in Table 1, using the $Ge_4$ analysis as a reference ($Ge_4$ was chosen as the reference because it represents a single $[Ge_4S_{10}]^{4-}$ cluster and because the Ge analyses are more reliable than the S analyses). From an average of eight samples prepared without sulfate, a Ge:S ratio of 4:9.4(8) was determined, in agreement with the ratio of 4:10 expected if the $[Ge_4S_{10}]^{4-}$ clusters are intact. The ratio of M:$Ge_4$ varied between 1.1 and 3.8. Interestingly, the samples prepared with Zn, Co, and Ni had M:$Ge_4$ analyses that were close to or less than the value expected from the synthesis. Cu, however, was unique in that a much higher than expected Cu:$Ge_4$ ratio was observed, which was nearly double all other M:$Ge_4$ values. Because the Cu:$Ge_4$ ratio was double other M:$Ge_4$ ratios, a $[Cu_2]^{2+}$ dimer may link the $[Ge_4S_{10}]^{4-}$ clusters in this material. This is reminiscent of the microporous $TMA_2Cu_2Ge_4S_{10}$ materials that contain a $[Cu_2]^{2+}$ dimer linking the adamantanoid clusters.[11] C and N analyses of the materials indicated that they contained approximately 2.2−2.5 CTA cations per $Ge_4$. Analysis of a CPM-Zn/$Ge_4S_{10}$ sample indicated a CPM:$Ge_4$ ratio of 1.83.

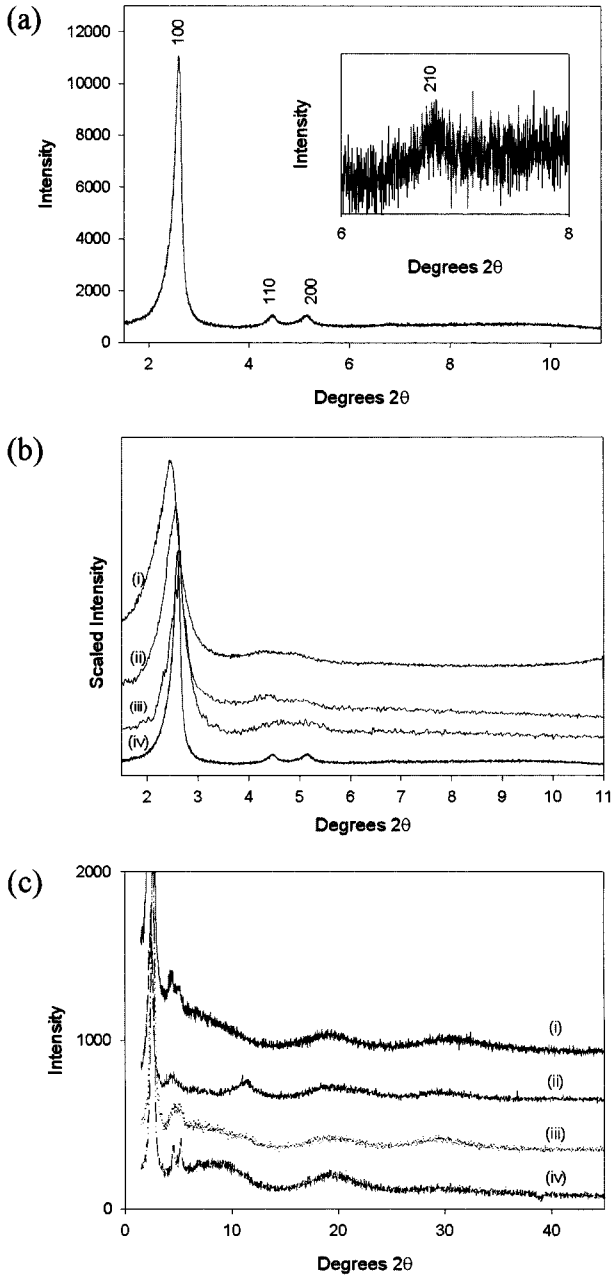


**Figure 1.** (a) PXRD pattern of CTA−Ni/$Ge_4S_{10}$ (with expanded region in the inset) in the low 2$\theta$ region showing four peaks diagnostic of hexagonal symmetry. (b) PXRD patterns of CTA−M/$Ge_4S_{10}$ (M = (i) Co, (ii) Cu, (iii) Zn, and (iv) Ni) in the low 2$\theta$ region also showing hexagonal symmetry. (c) In the high 2$\theta$ region, PXRD patterns of CTA−M/$Ge_4S_{10}$ (M = (i) Cu, (ii) Co, (iii) Zn, (iv) Ni) showing only broad, amorphous halos.

**Table 2.** Measured and Calculated Reflections for CTA−Ni/$Ge_4S_{10}$ on the Basis of a Unit Cell with $a_o$ = 39.45 Å

| refl | obs (Å) | calcd (Å) |
|---|---|---|
| $d_{100}$ | 34.18(1) | 34.18 |
| $d_{110}$ | 19.75(8) | 19.73 |
| $d_{200}$ | 17.19(8) | 17.09 |
| $d_{210}$ | 13.0(5) | 12.92 |

Three *meso*-Zn/$Ge_4S_{10}$ samples were analyzed for $Cl^-$, $Br^-$, and $H_2O$. There was essentially no halide present in the samples. This is surprising because a large amount of halide was used in the preparations. Water analyses of the samples indicated that they contained 3−8% moisture by mass.

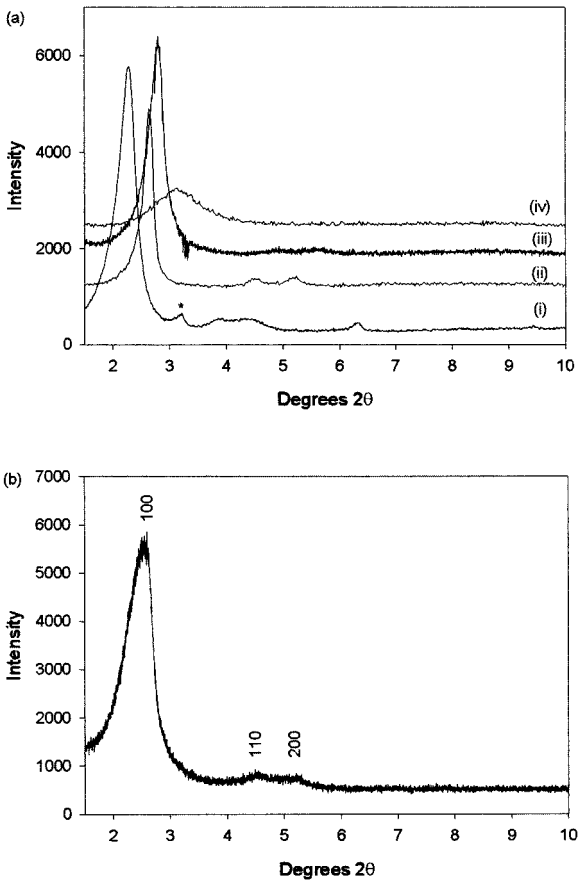


**Figure 2.** (a) PXRD patterns of meso-Ni/$Ge_4S_{10}$ prepared with surfactants $C_nH_{2n+1}NMe_3^+$ ($n$ = (i) 18, (ii) 16, (iii) 14, and (iv) 12) showing that the unit cell dimensions of the mesostructured material can be controlled by changing the length of the aliphatic hydrocarbon chain on the surfactant. (Note: the peak indicated by * is a small (ca. < 2%) impurity of a lamellar phase.) (b) PXRD pattern of CPM-Zn/$Ge_4S_{10}$ showing reflections characteristic of hexagonal symmetry.

**Table 3.** Effect of Surfactant Chain Length on Observed Reflections for Mesostructured Ni/$Ge_4S_{10}$ Materials and Comparison of the Calculated Unit Cell Parameters with the Unit Cell Determined for Mesoporous Silica, MCM-41

| surfactant chain length[a] | observed reflections from PXRD[b] | | | | hexagonal unit cell parameter[b] | |
|---|---|---|---|---|---|---|
| $n$ | $d_{100}$ | $d_{110}$ | $d_{200}$ | $d_{210}$ | $a_o$[c] | MCM-41$a_o$ |
| 12 | 28.1 | | | | 32.4 | 33[d] |
| 14 | 31.6 | 18.0 | 15.8 | | 36.5 | 38[d] |
| 16 | 34.2 | 19.7 | 17.2 | 13.0 | 39.5 | 40[d] |
| 18 | 38.9 | 22.8 | 20.2 | | 44.9 | |

[a] Surfactant was $C_nH_{2n+1}NMe_3^+X^-$ (X = Cl or Br). [b] In angstroms. [c] $a_o = 2d_{100}/(3)^{1/2}$ for hexagonal unit cell. [d] Surfactant removed; see Beck et al.[13]

The mesostructured products were characterized by several techniques to confirm the molecular and supramolecular structures of the materials. Visibly, the materials appeared distinctly colored depending on the metal incorporated. The materials were light green, deep green, white, and brown when Cu(I), Co(II), Zn(II), and Ni(II) were used, respectively. Interestingly, the materials did not have a sulfide odor, characteristic of volatile sulfur compounds discharged from other metal sulfides we have investigated.

**Powder X-ray Diffraction.** PXRD of the mesostructured materials typically showed two to four peaks consistent with a hexagonal unit cell. Often the (110) and (200) reflections overlapped in the diffraction patterns, possibly due to broadening

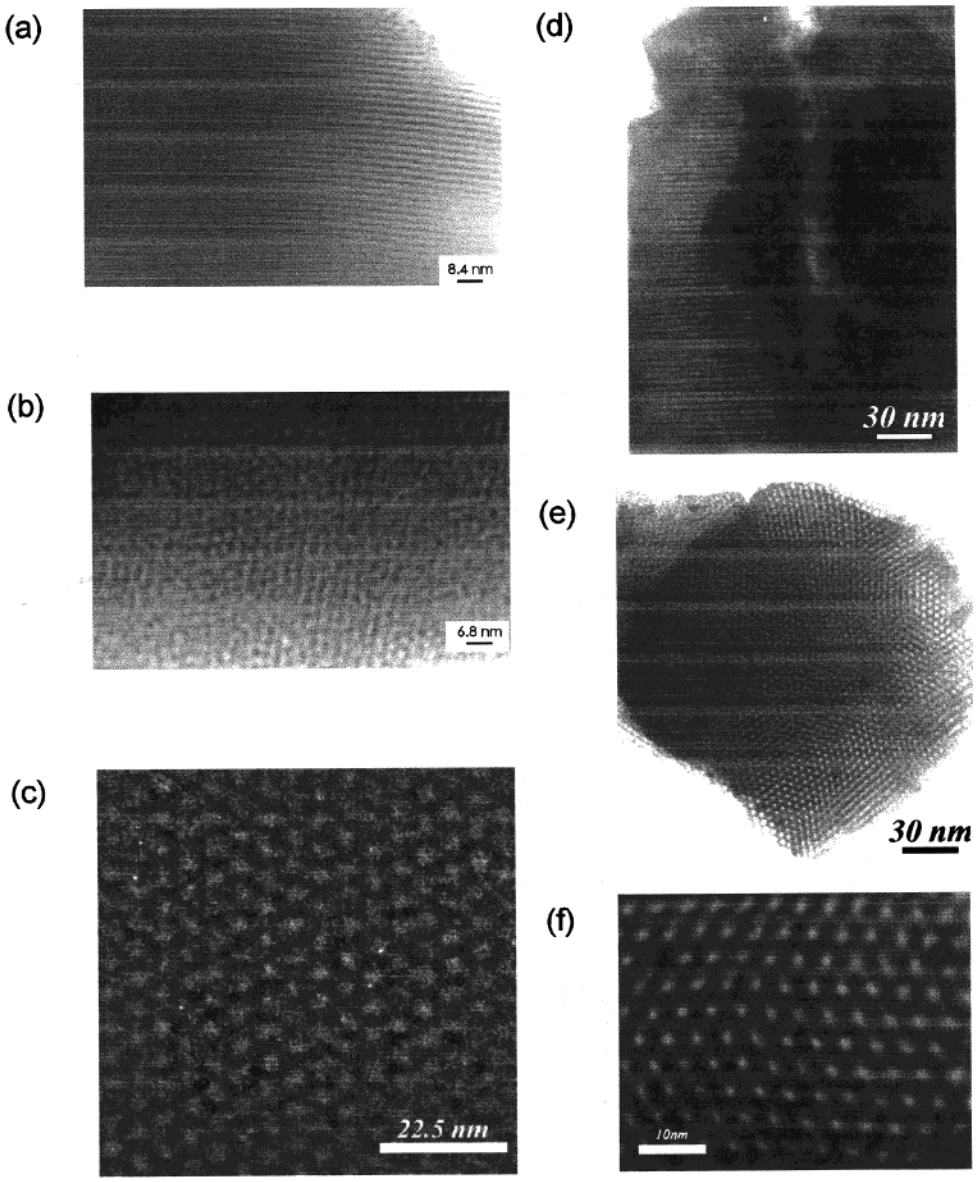


**Figure 3.** (a) TEM images of (a) CTA−Ni/$Ge_4S_{10}$ parallel to the channel axis, (b) CTA−Ni/$Ge_4S_{10}$ perpendicular to the channel axis, (c) CTA−Cu/$Ge_4S_{10}$ perpendicular to the channel axis, (d) CTA−Co/$Ge_4S_{10}$ parallel to the channel axis, and (e) CTA−Co/$Ge_4S_{10}$ perpendicular to the channel axis. (f) Expanded view of the hexagonal mesostructure in CTA−Co/$Ge_4S_{10}$.

associated with small particle sizes. Figure 1a shows a PXRD pattern of CTA−Ni/$Ge_4S_{10}$, where four peaks assigned to reflections from a hexagonal lattice with a unit cell dimension, $a_o$, of 39.5 Å were observed (Table 2). For comparison, $a_o$ observed for MCM-41 with a $C_{16}$ chain is 40 Å. The observation of four peaks is unusual for reported hexagonal mesostructured materials (besides silica) and attests to the high degree of order in the solid (confirmed by TEM; see later). In Figure 1b, the PXRD patterns of CTA−M/$Ge_4S_{10}$ (M = $Cu^+$, $Zn^{2+}$, $Co^{2+}$, $Ni^{2+}$) are characteristic of hexagonal symmetry. In addition to the diffraction peaks, several broad, amorphous halos were apparent in the materials, as illustrated in Figure 1c. These correspond to the most probable interatomic distances in the material.

The channel dimensions of MCM-41 can be tailored by choice of surfactant or by swelling an organic species (e.g., mesitylene) in the preformed liquid crystalline template.[13] To determine the effect of modifying the length of the surfactant's aliphatic hydrocarbon chain in the formation of the mesostructured metal germanium sulfides, *meso*-Ni/$Ge_4S_{10}$ materials were prepared with $C_nH_{2n+1}NMe_3^+X^-$ ($n$ = 12, 14, 16, 18) surfactants. PXRD patterns of the synthesized materials are displayed in Figure 2a. The degrees of order in the samples prepared with $n$ = 14, 16, and 18 were similar, showing an intense peak corresponding to the (100) reflection plus two to three additional reflections consistent with hexagonal symmetry. Samples prepared with dodecyltrimethylammonium ($n$ = 12) as surfactant were less well ordered, showing only a single peak, which was less intense. Samples prepared with $C_{18}H_{37}NMe_3^+$ also contained a small fraction of a lamellar phase, $d_{100}$ = 27.7 Å (est. <2% from integration of the $(100)_{lam}$:$(100)_{hex}$ reflections).

The materials display mesoscopic order with an increasing value of $d_{100}$ as the hydrocarbon chain length increased. Measured $d$ spacings of the reflections, the calculated hexagonal unit cell dimension, and the corresponding unit cell dimension reported for mesoporous silica are listed in Table 3. The unit cell dimensions nearly correspond with the values observed in MCM-41 templated with the same surfactants. When mesitylene was introduced into preparations, mesostructured materials were obtained. However, these materials showed diminished order (by PXRD) compared to materials prepared without mesitylene,

and the $d_{100}$ position did not change with the mole ratio of mesitylene:CTABr up to 1:1.

Other surfactants also gave well-ordered mesostructured materials with hexagonal symmetry. Figure 2b shows the PXRD pattern of CPM−Zn/$Ge_4S_{10}$ between 1 and 10° 2$\theta$. Three peaks associated with the hexagonal order of the material are clearly apparent. The lattice dimension of the mesostructure ($a_o \sim 40$ Å) is similar to that obtained with the surfactant CTABr.

The mesostructured metal germanium sulfides are remarkably stable over time. PXRD was performed on several samples that had been stored for more than a year under ambient conditions in the laboratory. The patterns of the aged and fresh samples were virtually identical and indicated no decrease in mesoscopic order in the samples.

**Transmission Electron Microscopy (TEM).** Samples of the mesostructured metal germanium sulfides were examined by TEM. Because the materials were unstable in the epoxy used to support the sample for microtoming, whole-mounted samples were used instead. This placed stringent demands on the observation of the mesostructure because the order was required to extend throughout the length of the particle between the electron beam and the detector. Survey of the samples showed that most of the particles were well-ordered (very little amorphous material was observed) and no dense phases were apparent by TEM. Energy-dispersive X-ray (EDX) analysis of single particles indicated that they contained Ge, S, and the expected metal. There is a large contrast between the metal germanium sulfide channel walls and the surfactant filling the pores. Figure 3a shows a view of CTA−Ni/$Ge_4S_{10}$ parallel to the channel axis. A TEM micrograph of the CTA−Ni/$Ge_4S_{10}$, observed perpendicular to the channel axis of the material, is shown in Figure 3b. The interpore spacing of approximately 40 Å is in agreement with the value calculated from the diffraction pattern, $a_o \sim 39.5$ Å. The hexagonal order of CTA−Cu/$Ge_4S_{10}$ is illustrated in Figure 3c. From the TEM micrograph, the interpore spacing is ca. 48 Å, close to the value of 40 Å expected from the PXRD pattern ($d_{100} = 34.5$ Å for this sample). The thick channel wall (15−20 Å) visualized in the TEM image is an artifact of using whole-mounted thick samples because any curvature of the channels is projected onto the image. Parts d and e of Figure 3 show images of the mesostructured CTA−Co/$Ge_4S_{10}$ material parallel and perpendicular to the channel axis, respectively. Again, the interpore spacing is consistent with the value measured by PXRD. A region of the image in Figure 3e is expanded in Figure 3f to illustrate clearly the hexagonal mesostructure.

TEM images of single particles show wormlike morphologies that are similar to those observed in MCM-41 (Figure 4).[20] The hexagonal mesostructure of the material is reflected in the morphology of the resultant material, where the particles have a large aspect ratio. Some of the particles even show facets, characteristic of a hexagonal unit cell. TEM images of the wormlike particles at higher magnification confirmed that the channels ran parallel to the length of the worm.

**Infrared Spectroscopy.** IR spectra of the mesostructured metal germanium sulfides prepared with the same surfactant and transition metal were very similar. The spectra showed many of the same modes as the crystalline surfactant (CTABr, CPMCl, and so on), but the peaks had significantly different intensities and line widths in the composite materials. Moreover, many of the peaks were substantially shifted from the surfactant. Figure 5 shows the IR spectra of CTA−Co/$Ge_4S_{10}$ and crystalline CTABr for comparison.

(20) Yang, H.; Coombs, N.; Ozin, G. A. *Nature* **1997**, *386*, 692.

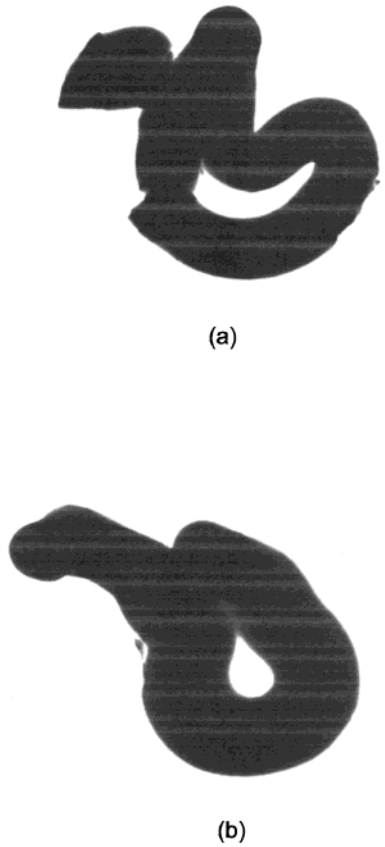


**Figure 4.** TEM images of wormlike particles of CTA−Ni/$Ge_4S_{10}$. A magnified view of the particle in image b confirmed that the channels of the material run parallel to the longitudinal axis of the faceted shape.

In addition to showing evidence for the surfactant, the IR spectra also showed the presence of water in all of the samples. An intense peak in the region of 3200−3500 $cm^{-1}$ was characteristic of O−H stretching. This peak often showed fine structure that could arise from the presence of coordinated and physisorbed water. In the region of 1600−1680 $cm^{-1}$, one or two modes were observed in the samples. These are probably bending modes associated with coordinated and physisorbed water. In most of the samples, broad low-frequency modes (ca. 1110 and 800 $cm^{-1}$) were also observed, and their intensity appeared to scale with the other peaks associated with water. The former may be assigned to a MOH bending mode of hydroxyl species and the latter to a deformation mode of coordinated water. No evidence for S−H stretching modes were observed in the IR spectra of the materials, although this mode is usually a weak band in the IR.

The IR spectra were also examined for the signature modes of formamide and anions that were present in the preparation. Although the NH stretching mode of formamide might be at a frequency similar to that of the O−H stretch for water and the carbonyl stretching mode might overlap with the bending mode for water, no characteristic C−H stretching mode for an aldehyde was observed. Samples prepared with $Ni(NO_3)_2$ showed no intense mode in the region 1380−1350 $cm^{-1}$ that would be characteristic of coordinated nitrates.[21] However, the samples prepared with $CoSO_4$ did show the presence of the anion, as indicated by an S−O stretching mode near 1100 $cm^{-1}$. In one sample, three bands were clearly resolved, indicating low site symmetry for the sulfate.

**Raman Spectroscopy.** Raman spectra of the mesostructured metal germanium sulfides (M = Co, Cu, Ni) could not be

(21) Bellamy, L. J. *The Infrared Spectra of Complex Molecules*; Chapman and Hall: New York, 1986; Vol. 1.

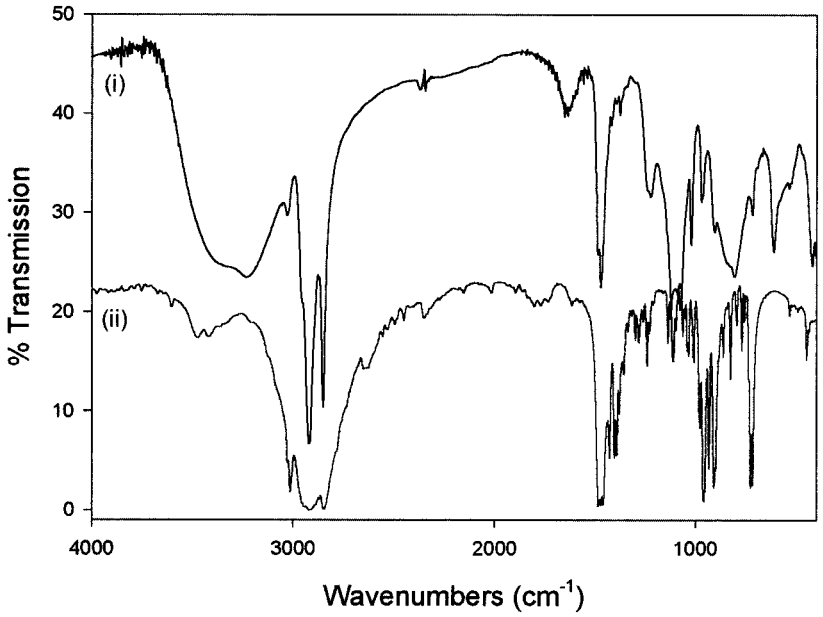


**Figure 5.** IR spectra of (i) CTA−Co/$Ge_4S_{10}$ and (ii) crystalline CTABr.

obtained as they decomposed under the laser radiation. However, Raman spectra of *meso*-Zn/$Ge_4S_{10}$ materials were obtained and proved essential to understanding the bonding in the materials. Figure 6a shows the Raman spectrum of CTA−Zn/$Ge_4S_{10}$ and CTABr for comparison. The Raman spectrum of CTA−Zn/$Ge_4S_{10}$ shows most of the modes characteristic of CTABr, but the peaks are generally broader and the intensities differ from pure CTABr. These observations are consistent with the presence of $CTA^+$ cations, in a distribution of environments, inside the mesostructured material.

Below 600 $cm^{-1}$, the Raman spectrum of CTA−Zn/$Ge_4S_{10}$ differs significantly from the spectrum of CTABr. This region, which is expanded in Figure 6b, bears the $\nu$Ge−S and $\nu$Zn−S modes that are not present in the pure surfactant. For comparison, the spectra of microporous, crystalline $TMA_2ZnGe_4S_{10}$ and lamellar $CTA_4Ge_4S_{10}$ are provided. The spectrum of $CTA_4Ge_4S_{10}$, in which the adamantanoid $[Ge_4S_{10}]^{4-}$ clusters are unconnected, displays two sets of peaks that are assigned to terminal $\nu$Ge−$S_t$ modes (340−480 $cm^{-1}$) and bridging $\nu$Ge−$S_b$ modes. The symmetric $\nu$Ge−$S_t$ mode is observed at 342.0 (±0.1) $cm^{-1}$ with a full width at half-maximum (fwhm) of 7.6 (±0.6) $cm^{-1}$. In the Raman spectrum of $TMA_2ZnGe_4S_{10}$, where all of the $[Ge_4S_{10}]^{4-}$ clusters are intact and linked to the tetrahedral metal centers, the symmetric mode has shifted to 350.7 (±0.2) $cm^{-1}$, but the line width is virtually unchanged (fwhm = 8.8 (±0.5) $cm^{-1}$). Weak modes attributed to $\nu$Zn−S stretching modes are present between 250 and 320 $cm^{-1}$. The Raman spectrum of CTA−Zn/$Ge_4S_{10}$ strongly resembles the spectrum of the microporous $TMA_2ZnGe_4S_{10}$ framework in the $\nu$Ge−S region, but the peaks are much broader. The symmetric $\nu$Ge−S mode is observed at 350.7 (±0.2) $cm^{-1}$ in CTA−Zn/$Ge_4S_{10}$, diagnostic of metal-linked clusters. This peak is substantially broader (fwhm = 19 (±2) $cm^{-1}$) than that of the symmetric $\nu$Ge−$S_t$ mode of the crystalline $CTA_4Ge_4S_{10}$ and $TMA_2ZnGe_4S_{10}$ materials. The region between 240 and 320 $cm^{-1}$ contains many $\nu$Zn−S stretching modes, as observed in the metal-linked, microporous $TMA_2ZnGe_4S_{10}$ materials.

The Raman spectrum of CPM−Zn/$Ge_4S_{10}$ is very similar to the spectrum for CTA−Zn/$Ge_4S_{10}$ between 600 and 100 $cm^{-1}$ (Figure 6c). As with the other metal-linked materials, the symmetric $\nu$Ge−$S_t$ mode is shifted to ca. 350 $cm^{-1}$ and broadened relative to $CTA_4Ge_4S_{10}$ and $TMA_2ZnGe_4S_{10}$. Moreover, a congested region of $\nu$Zn−S modes is present between 240 and 320 $cm^{-1}$ in the mesostructured CPM−Zn/$Ge_4S_{10}$ material.

Raman spectra of the mesostructured solids are consistent with the presence of metal-linked $[Ge_4S_{10}]^{4-}$ clusters present in a number of sites, where the variation in the coordination environment may lead to the increased Raman line width of the Ge−S modes. Notably, the adamantanoid $[Ge_4S_{10}]^{4-}$ clusters are still intact in the materials, in agreement with the Ge:S ratio determined by elemental analysis. Moreover, no evidence for thiol groups ($\nu$S−H) was observed in the samples.

**Reflectance UV−vis/Near-IR Spectroscopy.** The optical spectroscopy of microporous $TMA_2MGe_4S_{10}$ materials has been investigated previously.[11,22,23] The precursor, $TMA_4Ge_4S_{10}$, shows only an intense highest occupied (HOMO) to lowest unoccupied molecular orbital (LUMO) transition in the UV region that begins at ca. 375 nm with a maximum at 330 nm. As metals are introduced, d−d transitions are observed, and the optical spectra are strongly dependent on the metal. The microporous frameworks $TMA_2ZnGe_4S_{10}$ and $TMA_2Cu_2Ge_4S_{10}$ showed no d−d absorptions as they are both $d^{10}$ systems.[22] In $TMA_2CoGe_4S_{10}$, however, the metal is in a distorted tetrahedral environment with vacant d orbitals; so, d−d absorptions in the visible and near-IR regions were observed.[22] Moreover, each of the materials showed an intense absorption near 350 $cm^{-1}$ that is assigned to a ligand-to-metal charge-transfer (LMCT) band. The position of this band is also dependent on the identity of the transition metal.

Two samples of each CTA−M/$Ge_4S_{10}$ (M = $Zn^{2+}$, $Cu^+$, $Co^{2+}$, $Ni^{2+}$) were investigated by reflectance UV−vis/near-IR spectroscopy between 200 and 2500 nm. The spectra of different samples prepared with the same metal were remarkably similar. The spectra for each of the materials CTA−M/$Ge_4S_{10}$, shown in Figure 7, will be discussed in turn.

The near-IR region of the spectrum of CTA−Zn/$Ge_4S_{10}$ shows several weak peaks that may be assigned to overtones and combinations of the IR modes of the surfactant and water in the sample. As expected for a $d^{10}$ system, there are no

(22) Kirkby, S. J. *Spectroscopy and Crystallography of Metal Germanium Chalcogenide Framework Materials and Precursors*, Ph.D. Thesis, University of Toronto, 1996.

(23) Kirkby, S. J.; Ozin, G. A. *Mater. Res. Symp. Proc.* **1996**, *431*, 165.

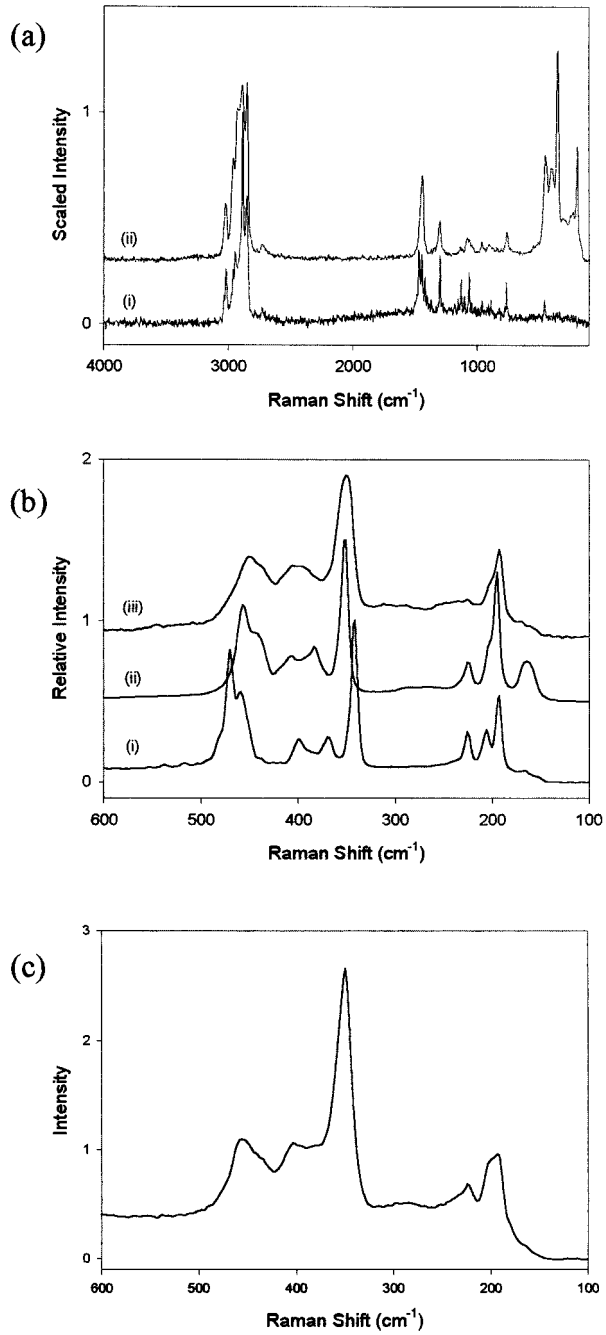


**Figure 6.** (a) Raman spectra of (i) CTABr and (ii) CTA−Zn/$Ge_4S_{10}$. (b) Raman spectra of (i) $CTA_4Ge_4S_{10}$, (ii) $TMA_2ZnGe_4S_{10}$, and (iii) CTA−Zn/$Ge_4S_{10}$ in the region 600−100 $cm^{-1}$ where $\nu$Ge−S and $\nu$Zn−S modes are observed. (c) Raman spectrum of CPM−Zn/$Ge_4S_{10}$ between 600 and 100 $cm^{-1}$.

absorptions in the visible portion of the spectrum. In the UV region, an absorption edge begins at ca. 450 nm and peaks at 300 nm. This is shifted slightly from the precursor, $TMA_4Ge_4S_{10}$, which shows an absorption edge beginning at ca. 375 nm with a maximum at 330 nm.

The spectrum for Co showed peaks in the near-IR between 2260 and 2370 nm that can be assigned to combination modes of adsorbed water. Between ca. 1100 and 2200 nm, an intense near-IR absorption was observed that appears to consist of two or more transitions when fitted to Gaussian curves. An optical transition in the visible portion of the spectrum between ca. 600 and 900 nm (peak at 720 nm) shows fine structure consistent with multiple overlapping peaks. A fit to Gaussian curves

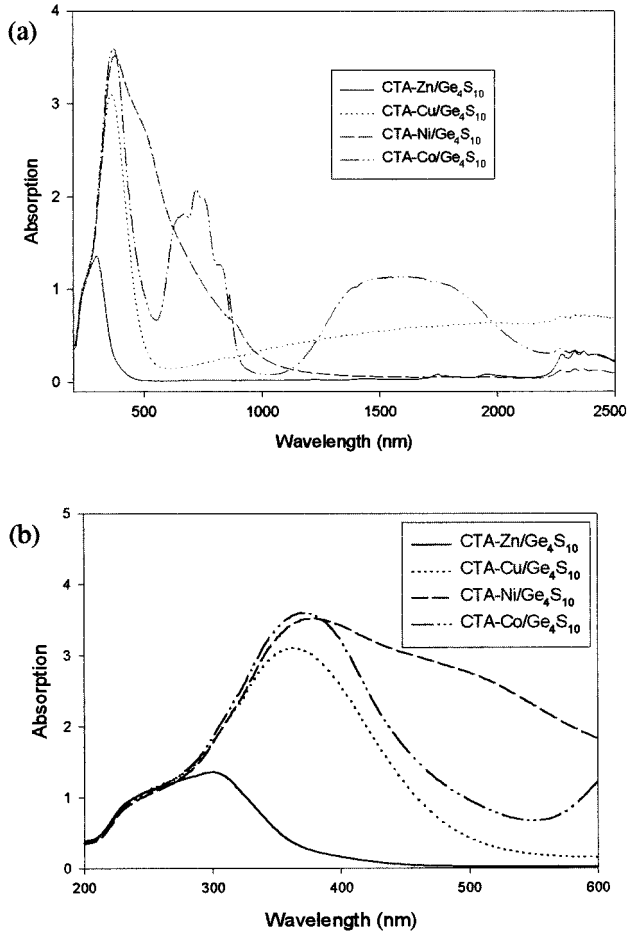


**Figure 7.** (a) Reflectance UV−vis/near-IR spectra of the mesostructured metal germanium sulfides CTA−M/$Ge_4S_{10}$. (b) UV−vis absorption spectra for the same materials between 200 and 600 nm.

suggested that there are at least five overlapping peaks from 640 to 820 nm. An absorption edge beginning at ca. 600 nm shows a maximum at 367 nm. Deconvolution of this peak indicated the presence of at least two peaks: 362 and 269 nm. The former band might be assigned to ligand-to-metal charge transfer.

Co(II) is a $d^7$ ion, giving rise to eight terms in which $^4P$ and $^4F$ are the terms with highest spin multiplicity. In a tetrahedral environment, the $^4P$ term has $^4T_1$ symmetry, and the free ion ground term ($^4F$) is split into $^4A_2$, $^4T_1$, and $^4T_2$ terms, with $^4A_2$ being the ground state. This gives rise to three expected transitions ($^4T_2 \leftarrow {}^4A_2$, $^4T_1(F) \leftarrow {}^4A_2$, and $^4T_1(P) \leftarrow {}^4A_2$), which generally occur in the visible and near-IR regions.[24] In the microporous $TMA_2CoGe_4S_{10}$ frameworks, where the Co is coordinated by four sulfide ligands, these transitions were observed in the regions of 2000, 1400, and 700 nm. Kirkby deduced that splitting of the absorption near 700 nm was characteristic of a distorted tetrahedral environment.[22] In the mesostructured CTA−Co/$Ge_4S_{10}$ materials, broad regions of overlapping bands centered near 700 and 1600 nm suggest that the Co has a microenvironment similar to Co in the microporous framework. The presence of defect sites (e.g., where Co is coordinated by water or sulfate instead of sulfide at one coordination site), which would result in a change in the orbital splitting, could be responsible for the breadth of these transitions.

It is interesting that Ni forms a very well ordered mesostructured framework but has proved difficult to form the

(24) Greenwood, N. N.; Earnshaw, A. *Chemistry of the Elements*; Butterworth-Heinemann: Oxford, 1997; p 1132.

analogous microporous framework. In the reflectance spectrum, several modes were observed between 1690 and 2500 nm. They are nearly the same as those observed in the CTA−Zn/$Ge_4S_{10}$ material and can be assigned to combination and overtone modes of the surfactant and water. A very broad absorption edge began at ca. 1200 nm, spanned the entire visible spectrum (hence the brown color of the material), and peaked at 380 nm. The absorption fit quite well to five Gaussian peaks centered at ca. 750, 670, 460, 357, and 246 nm. The first three transitions are assigned to d−d transitions of the Ni (note that they are very broad and there may be many more contributing peaks), and the peak at 357 nm may be a LMCT band.

Ni(II) is a $d^8$ metal. In a tetrahedral field, three fairly intense bands would be expected, with a $^3A_2 \leftarrow {}^3T_1(F)$ transition typically detected in the near-IR (ca. 1400 nm).[25] The absence of a peak in this region strongly suggests that the Ni(II) in the mesostructured material is not in a tetrahedral geometry. All of the absorption bands in octahedral and square-planar Ni(II) are typically observed at high energy. Thus, these two geometries are the most likely candidates.

It seems highly unlikely that Ni(II) would coordinate to six $[Ge_4S_{10}]^{4-}$ clusters due to steric interactions. Many nickel tetrathiolate complexes are found in a square-planar geometry.[26] The possibility of octahedral or 5-coordinate Ni centers where some of the coordination sites are occupied by solvent or anions cannot be excluded.

Reflectance UV−vis/near-IR spectroscopy of the microstructured $TMA_2Cu_2Ge_4S_{10}$ framework showed no transitions in the near-IR or visible region, but did show an absorption edge rising from ca. 550 nm and peaking near 360 nm.[22] This optical transition was observed in the mesostructured CTA−Cu/$Ge_4S_{10}$ materials, rising from 550 nm and peaking at 365 nm. A weak band was also observed at 238 nm.

In the near-IR region, however, the spectrum of the mesostructured framework is distinct from the microstructured material. Weak overtone/combination modes were observed at 2280−2370 nm. A very broad, intense transition extending from about 600 nm to over 2500 nm, with its center near 2000 nm, dominated the near-IR portion of the spectrum. Broad, intense near-IR absorptions similar to this have been observed in mixed valence Cu(I)/Cu(II) dimers.[27]

**Magnetic Susceptibility Measurements.** Room temperature magnetic susceptibilities were obtained for samples of CTA−M/$Ge_4S_{10}$ (M = Cu, Co, Zn, Ni). For the purpose of estimating the magnetization on each metal center, an approximate formula of $CTA_2M_2Ge_4S_{10}$ was assumed (except for Cu, where a formula of $CTA_2Cu_4Ge_4S_{10}$ was used) in accord with those observed for analyzed samples.

As expected for a $d^{10}$ metal, the magnetic susceptibility of CTA−Zn/$Ge_4S_{10}$ indicated that it was diamagnetic. A sample of CTA−Co/$Ge_4S_{10}$ that was measured showed a magnetic susceptibility of 3.1 $\mu_B$. Given that there may be a substantial error associated with the ideal formula, which was assumed, this is not unreasonable for tetrahedral Co(II), which would be expected to possess three unpaired electrons and, thus, a have a magnetic moment of 3.87 $\mu_B$ (neglecting orbital contribution).

Two samples of CTA−Cu/$Ge_4S_{10}$ showed very weak magnetic susceptibilities (average 0.16 $\mu_B$). This suggests that most of the Cu is present as Cu(I), with a small population of Cu(II) centers present in the material. From the observation of a near-IR transition in the optical reflectance spectrum of both samples of CTA−Cu/$Ge_4S_{10}$, the Cu(II) most likely exists as Cu(I)−Cu(II) mixed-valence centers in a material that primarily contains Cu(I)−Cu(I) dimers.

The room temperature magnetic susceptibilities of two CTA−Ni/$Ge_4S_{10}$ samples were measured. They possessed magnetic moments of 1.35 and 1.82 $\mu_B$ per Ni, assuming the ideal formula. This is consistent with an average of one unpaired electron per Ni. We postulate that this results from a mixture of diamagnetic square-planar Ni(II) centers plus paramagnetic octahedral or square-pyramidal Ni(II). It is also possible that there are paramagnetic Ni(III) sites in the material, but the former agree more closely with the results of the optical spectroscopy.

**NMR Studies.** Solid-state $^1H$ MAS and $^{13}C$ CP-MAS NMR of CTA−Cu/$Ge_4S_{10}$, CTA−Zn/$Ge_4S_{10}$, and CPM-Zn/$Ge_4S_{10}$ confirmed the identity of the surfactant in the mesostructured materials. The $^1H$ spectra of the former two materials look virtually the same, showing two broad resonances for the hydrophobic carbon chain near 1 ppm and a broad resonance for the protons on the methyl and methylene groups adjacent to N. In CPM−Zn/$Ge_4S_{10}$, this latter resonance is much smaller as there are only two protons adjacent to N and a broad resonance has emerged near 8 ppm. $^{13}C$ NMR of the samples prepared with CTA and CPM (Figure 8) showed very sharp peaks. All of the peaks associated with the surfactant headgroups were observed as well as the aliphatic hydrocarbon chain.

Perhaps the most interesting aspect of the NMR spectra is the absence of resonances attributed to formamide ($^{13}C$ NMR, $\delta$ = 167 ppm). Because the samples were washed with formamide then water, the former solvent may have been removed from the samples. The $^1H$ MAS NMR resonance for water in the samples would likely overlap with the broad $NCH_2$/$NCH_3$ resonances observed at 3−4 ppm.

**Thermal Stability.** We investigated the thermal stability of the mesostructured metal germanium sulfides by thermogravimetric analysis (TGA), pyrolysis mass spectrometry, and VT-PXRD (for CTA−Cu/$Ge_4S_{10}$). All of the materials prepared with CTABr as the surfactant showed similar thermal properties. Figure 9a shows the TGA traces for samples of CTA−M/$Ge_4S_{10}$ (M = $Cu^+$, $Zn^{2+}$, $Ni^{2+}$, $Co^{2+}$) heated under $N_2$. Each of the samples showed a small weight loss (ca. 1−5 wt %) between room temperature and 150 °C, probably due to loss of physisorbed water from the material. Then, beginning at ca. 200 °C, each of the materials underwent a weight loss of ca. 50 wt % up to 500 °C. This weight loss occurs at nearly the same temperature as surfactant decomposition in the channels of MCM-41. Figure 9b shows the TGA trace for CTA−Ni/$Ge_4S_{10}$ along with the differential TGA trace. Pyrolysis mass spectrometry indicated that all weight loss corresponded to the decomposition of the surfactant. $Me_2NCH_2^+$ and $C_{16}H_{33}NMe_2^+$ were the major decomposition products observed in the mass spectrometer. Water and fragments of the surfactant, distinguished by a progression of $CH_2$ losses, were also observed. Notably, no S-containing compounds such as $H_2S$, HSMe, and $Me_2S$ were observed in the mass spectra. This is in contrast to $TMA_2MGe_4S_{10}$ frameworks that undergo decomposition via elimination of $Me_2S$ and $NMe_3$.[9a,11] Thus, the decomposition of the mesostructured frameworks occurs through a different mechanism than that in the microstructured GS-3 materials.

The distinction may be traced to the existence of coordinatively unsaturated sites around the transition metals that connect

(25) Greenwood, N. N.; Earnshaw, A. *Chemistry of the Elements*; Butterworth-Heinemann: Oxford, 1997; p 1158.

(26) Wilkinson, G., Ed. *Comprehensive Coordination Chemistry*; Permagon: Toronto, 1987; Vol. 5, p 166.

(27) (a) Wilkinson, G., Ed. *Comprehensive Coordination Chemistry*; Permagon: Toronto, 1987; Vol. 5, p 586. (b) Getteschi, D.; Mealli, C.; Sacconi, L. *Inorg. Chem.* **1976**, *15*, 2774. (c) Harding, C.; McKee, V.; Nelson, J. *J. Am. Chem. Soc.* **1991**, *113*, 9684.

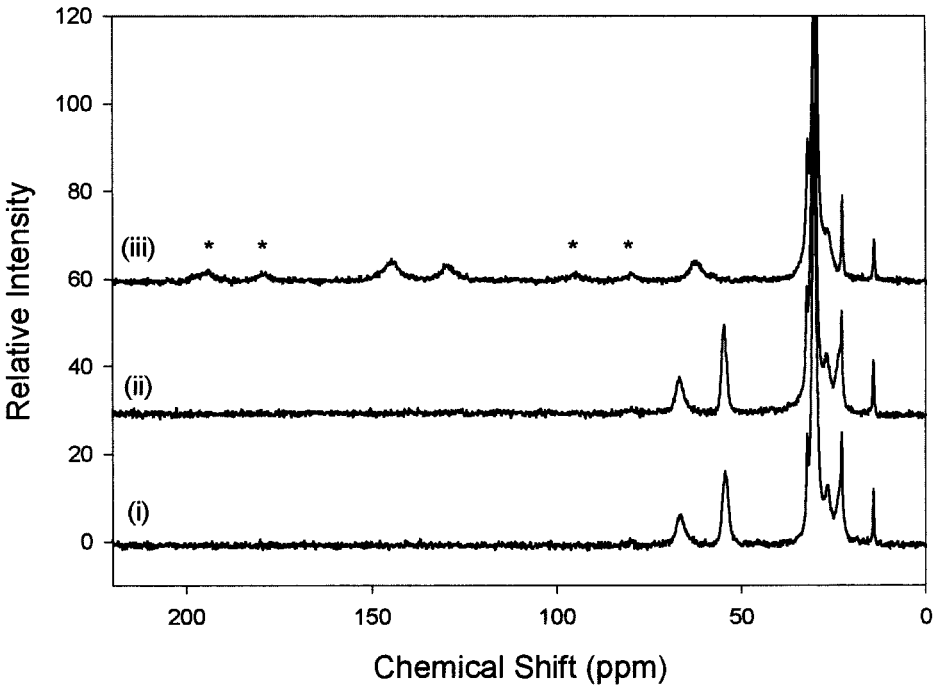


**Figure 8.** $^{13}$C CP-MAS NMR spectra of (i) CTA−Cu/$Ge_4S_{10}$, (ii) CTA−Zn/$Ge_4S_{10}$, and (iii) CPM−Zn/$Ge_4S_{10}$. (Spinning sidebands are marked with *)

$[Ge_4S_{10}]^{4-}$ building blocks in the mesostructure. These metal sites may facilitate fragmentation reactions of the surfactant that are not possible in the microstructured framework, where the tetrahedrally coordinated metal sites are spatially more congested.

Mesostructured CTA−Cu/$Ge_4S_{10}$ was examined by VT-PXRD under vacuum. Diffraction of the region 1−10° 2$\theta$ was monitored at 100, 150, and 200 °C and then every 20 °C from 200 to 400 °C. The PXRD patterns obtained are illustrated in Figure 10. Initially, three peaks were observed, with the most intense $d_{100}$ peak observed at $d$ = 33.2 Å. As the sample was heated, the material expanded slightly to $d_{100}$ = 33.6 Å at 200 °C. The order of the mesostructure was maintained as the full width at half-maximum (fwhm) of the $d_{100}$ reflection (0.41° 2$\theta$) was constant up to this temperature. Then, the material underwent a dramatic structural change between 200 °C and 400 °C. The (100), (110), and (200) reflections decreased in intensity, with the latter two completely absent after ca. 240 °C. The fwhm of the $d_{100}$ peak tended to increase from 200 to 400 °C, ending with a value of 1.1° 2$\theta$.

As the mesostructural organization of the CTA−Cu/$Ge_4S_{10}$ was lost, the material underwent a large contraction and $d_{100}$ decreased by a third between 200 and 400 °C. Figure 11 shows a graph of $d_{100}$ versus temperature and fwhm of the (100) reflection versus temperature. The contraction correlates well with the loss of surfactant observed by TGA. In addition, as indicated in Figure 11, there is a one-to-one correspondence between the decrease in the pore size (proportional to $d_{100}$) and the increase in fwhm. Clearly, loss of surfactant from the material results in contraction, and ultimately collapse, of the mesostructured metal germanium sulfides.

## Discussion

The absence of well-characterized non-oxide mesostructures in the literature inspired us to create a sulfide-based material like mesostructured silica, MCM-41. During our initial attempts to prepare mesostructured metal germanium sulfides, we encountered a solubility difficulty that prevented the synthesis of the materials in water, the conventional route to MCM-41 materials. We chose formamide as a solvent because it readily dissolved all of the starting materials and because phase diagrams of surfactants in formamide resemble those in water.[28]

The mesostructured inorganic−organic composites obtained show a high degree of order as manifested in the hexagonal symmetry of the PXRD patterns and TEM images of the materials. All of the samples visualized displayed hexagonal order extending over whole particles. Wormlike morphologies analogous to those observed in mesoporous silica were imaged in the metal germanium sulfides. Moreover, TGA, IR, and Raman spectroscopy of the materials indicated that they contained a similar proportion of surfactant to MCM-41. This implies that a similar growth process determines the form of these mesostructures.

Although the mesostructure of the metal germanium sulfides resembles MCM-41, the microstructure of the materials is very similar to those present in the microcrystalline GS-3 frameworks. Elemental analysis confirmed that the materials possessed a Ge:S ratio that is consistent with intact $[Ge_4S_{10}]^{4-}$ clusters. From the analyses, the materials appeared to possess a formula that was close to $(CTA)_2M_2Ge_4S_{10}$ (M = $Zn^{2+}$, $Co^{2+}$, $Ni^{2+}$, $Cu_2^{2+}$). We speculate that this stoichiometry could arise from the structure of the liquid crystalline assembly. For example, there may be two CTA molecules interacting closely with a single adamantanoid cluster, although we have no direct evidence for this. The remainder of the charge on the materials may be accounted for by the presence of anions such as hydroxyl groups or sulfate coordinated to the metals.

Raman spectra for the *meso*-Zn/$Ge_4S_{10}$ frameworks indicated that the $[Ge_4S_{10}]^{4-}$ clusters are present in environments similar to those in the microcrystalline GS-3 frameworks. Thus, the framework contains metal-to-sulfur bonds linking the clusters together. The breadth of the $\nu$Ge−S and $\nu$Zn−S modes indicate

(28) Wärnheim, T.; Jönsson, A. *J. Colloid Interface Sci.* **1988**, *125*, 627.

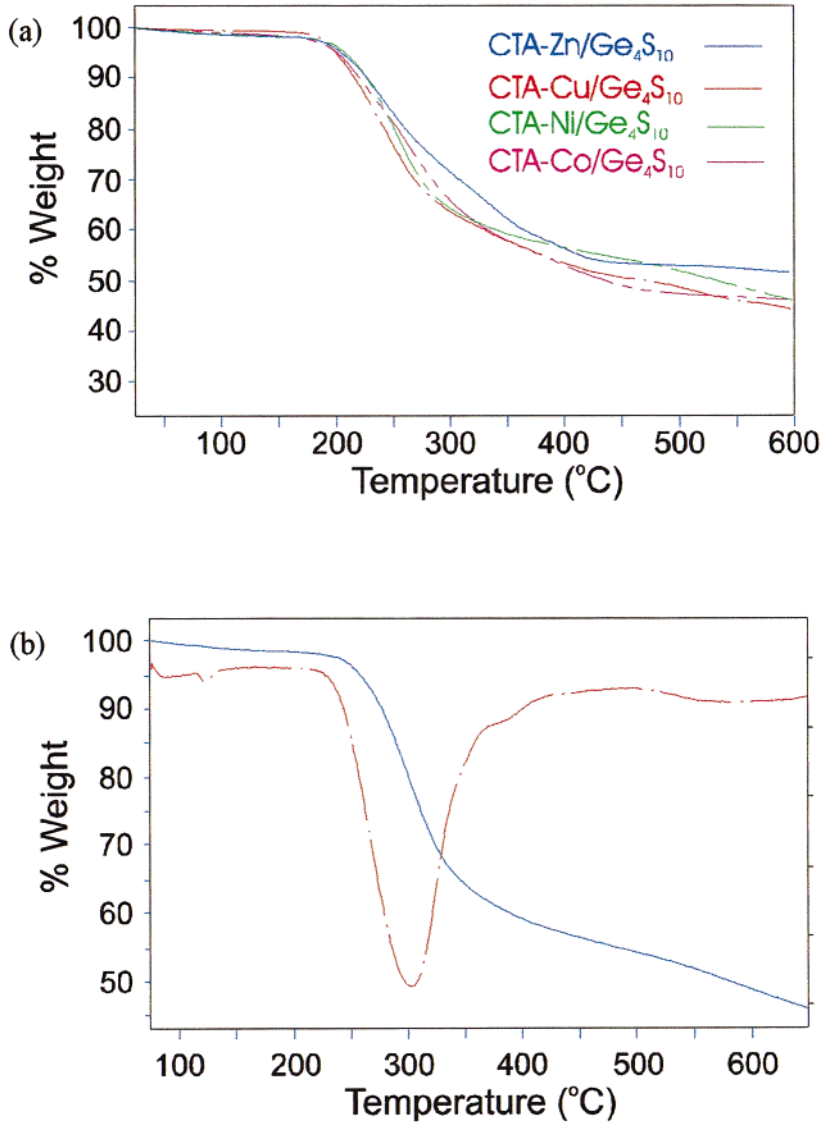


**Figure 9.** (a) TGA traces of the mesostructured metal germanium sulfides. (b) TGA (solid) and DTGA (dash−dot) traces for CTA−Ni/$Ge_4S_{10}$.

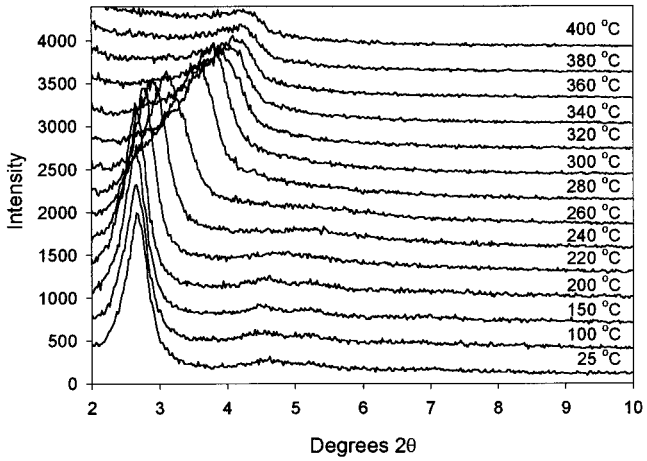


**Figure 10.** High-temperature PXRD patterns of CTA−Cu/$Ge_4S_{10}$ under vacuum. The temperatures at which the spectra were obtained are indicated.

that there is a distribution of environments present. IR spectroscopy confirmed that anions and water were present, which, if coordinated to the metal sites as defects in the place of sulfide ligands, would be expected to generate a distribution of metal sites. Anions such as sulfate and hydroxyl groups could balance the charge on the framework.

From the reflectance optical spectroscopy and room temperature magnetic susceptibility of the materials, it is clear that $Zn^{2+}$ and $Co^{2+}$ are in microenvironments similar to those observed in the GS-3 frameworks (distorted tetrahedral, $S_4$ site symmetry). The breadth of the absorption peaks in the CTA−Co/$Ge_4S_{10}$ spectrum is consistent with a distribution of microenvironments that might arise if solvent or anions were coordinated to the metals. The fact that the CTA−Co/$Ge_4S_{10}$ material changes color from blue to green upon washing with water is consistent with the presence of solvent coordinated to the Co(II) centers.

It is very interesting that Ni(II) forms a mesostructured metal germanium sulfide and that it appears to be the best ordered. To date, $Ni^{2+}$ has been noticeably absent from the list of GS-3 compositions prepared by the room temperature molecular assembly route developed by Yaghi. It should be noted, however, that the material has been prepared hydrothermally from $GeS_2$ by Bedard.[6,7] The reflectance spectrum of *meso*-Ni/$Ge_4S_{10}$ samples indicated that the Ni was not present in a tetrahedral environment, but more likely in a square planar geometry, possibly with water coordinated as well. Magnetic

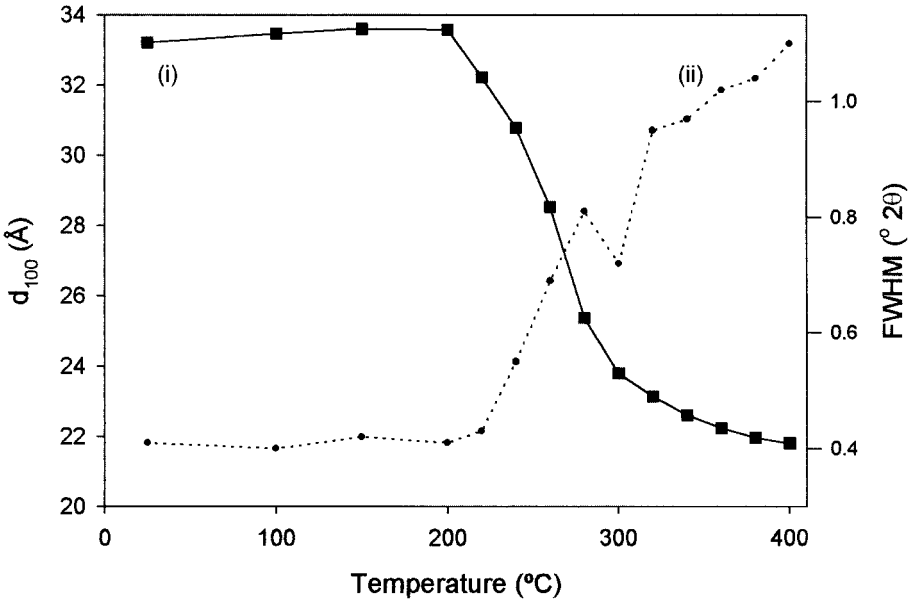


**Figure 11.** Graph of (i) $d_{100}$ vs temperature and (ii) fwhm of the (100) reflection vs temperature for CTA−Cu/$Ge_4S_{10}$. The material shows a concomitant contraction and loss of order above 200 °C.

susceptibility measurements confirmed that the Ni was not all square planar, which would be diamagnetic, but must also contain some octahedral or square-pyramidal Ni(II) centers. The resistance of Ni(II) to exhibit tetrahedral coordination in the presence of $[Ge_4S_{10}]^{4-}$ clusters may be the reason it will not form the microstructured GS-3 framework through the room temperature route.

None of the PXRD patterns of the mesostructured materials showed any other crystalline products (e.g., surfactant, $GeS_2$, GS-3 frameworks). When the syntheses were done in the absence of surfactant, crystalline microstructured GS-3 materials were obtained for $Fe^{2+}$, but no product formed for $Zn^{2+}$. This is in contrast to the same reaction in water, where $TMA_2$-$ZnGe_4S_{10}$ frameworks precipitate instantly from solution.

The presence of the transition metal is essential for formation of the products. If no transition metal was added, the solution remained clear and colorless at 80 °C for months. Attempts to form the mesostructured metal germanium sulfide framework with manganese, titanium, iron, and silver have been unsuccessful thus far. It is interesting that no product was obtained when manganese (II) acetate was added to the liquid crystalline assembly, although it readily forms microcrystalline metal germanium sulfides.[8] Kinetics of ligand displacement may be unfavorable in formamide, but this is only speculation. Kanatzidis recently showed that a mesostructured Mn/$Ge_4S_{10}$ material could in fact be prepared with a wormlike pore structure, through a high-temperature hydrothermal synthesis.[18b]

When $TMA_4Ge_4S_{10}$ is combined with CuCl in water, a microstructured metal germanium sulfide is obtained that contains $[Ge_4S_{10}]^{4-}$ clusters linked by $[Cu_2]^{2+}$ dimers as determined by a Rietveld structure solution.[11] It is therefore reasonable that mesostructured CTA−Cu/$Ge_4S_{10}$ could also possess a Cu−Cu bond. The elemental analysis of a CTA−Cu/$Ge_4S_{10}$ sample indicated that it contained approximately twice as much metal per $[Ge_4S_{10}]^{4-}$ cluster as that of the Zn and Co analogues, although substantially less Cu was used in the preparation. The mesostructured material is similar in color to the microstructured material: yellow-green. Mesostructured CTA−Cu/$Ge_4S_{10}$ showed no absorptions in the visible region but had an intense absorption in the UV at 361 nm. This corresponds well with the absorption edge observed in the microstructured $TMA_2Cu_2Ge_4S_{10}$ framework, ca. 360 nm. This transition has been previously assigned to a ligand-to-metal charge-transfer band.[22] In the near-IR spectrum of CTA−Cu/$Ge_4S_{10}$, an intense band was observed that may be due to an intervalence charge-transfer band for Cu(I)−Cu(II) dimers. Bands in this region have been observed for other systems.[27]

Magnetic susceptibility measurements indicated that most of the Cu is present as Cu(I) with a small amount of Cu(II), which may be present as Cu(I)−Cu(II) dimers. It is remarkable that the Cu remains in the +1 oxidation state, even when no care was taken to degas solvents or to perform the experiments under an inert atmosphere. There was no noticeable change to the materials after they were kept in air for several months.

A Cu-edge EXAFS experiment was performed on each of the *meso*-Cu/$Ge_4S_{10}$ and microstructured $TMA_2Cu_2Ge_4S_{10}$ materials.[29] Preliminary results suggest that both of the materials have very similar Cu environments. Small near-edge differences were consistent with the *meso*-Cu/$Ge_4S_{10}$ having a slightly higher average Cu oxidation state than that of the microstructured material. However, it has not yet been possible to fit the data to a suitable model. Our present characterization evidence, though indirect, suggests that the CTA−Cu/$Ge_4S_{10}$ material does contain metal−metal bonds in the mesostructured framework.

Like MCM-41, the mesostructured M/$Ge_4S_{10}$ materials may be prepared with a variety of surfactants. It should prove possible to modify the optical, electronic, and adsorptive properties of the materials by varying the surfactant (e.g., using metal-containing surfactants). Variation of surfactants can also be used to control the size of the pores in the resulting material. Preliminary experiments with mesitylene showed no pore expansion. In contrast to aqueous surfactants, where hydrophobic molecules are readily incorporated into the micellar region, our trials with mesitylene and other nonpolar molecules (e.g., decane, cyclohexane) indicated that the nonpolar species was immiscible with the surfactant assembly. This difference may result from the relative differences in the interfacial energy between nonpolar molecules and the solvent (water, formamide).[28]

(29) Bedard, R. L.; Bare, S.; MacLachlan, M. J.; Ozin, G. A., unpublished results.

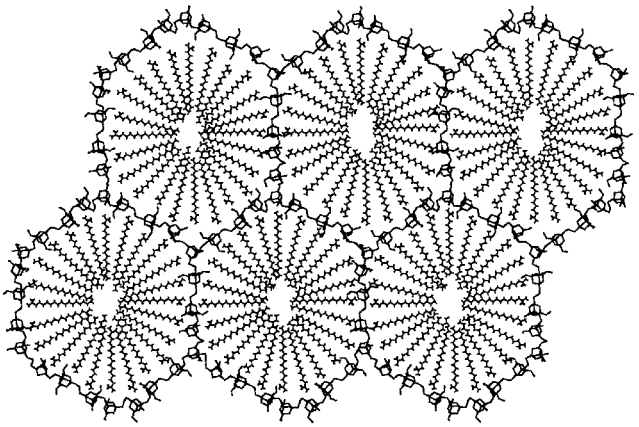

**Figure 12.** Idealized 2-D model of a mesostructured metal germanium sulfide showing the cluster-linked framework templated around the surfactant.

Our data suggests that the mesostructure of the *meso*-M/$Ge_4S_{10}$ materials is very similar to that of MCM-41 whereas the microstructure is similar to that of microcrystalline $TMA_2MGe_4S_{10}$ frameworks. We feel justified to explain the formation of the mesostructured metal germanium sulfides by a liquid-crystal templating mechanism that is analogous to the mechanism proposed for the formation of MCM-41.[13] First, $TMA_4Ge_4S_{10}$ and CTABr in formamide at 80 °C form a lyotropic inorganic liquid crystalline phase. In this liquid crystal, the hydrophobic chains of the surfactant are aggregated into cylindrical or micellar species with the $TMA^+$, $[Ge_4S_{10}]^{4-}$, and $Br^-$ in the solvent around the headgroups. As transition metals ($Co^{2+}$, $Cu^+$, $Zn^{2+}$, $Ni^{2+}$) are added, they are rapidly coordinated by the tetradentate $[Ge_4S_{10}]^{4-}$ clusters, "freezing" the M/$Ge_4S_{10}$ framework around the surfactant and immediately precipitating from solution. Figure 12 is a model of the proposed framework in which transition metals are linked to the adamantanoid $[Ge_4S_{10}]^{4-}$ clusters around a lyotropic liquid crystalline phase in formamide.

The thermal properties of the materials are worthy of further discussion. In contrast to the microstructured analogues, we think that the collapse of the mesostructure occurs by a physical transformation rather than a chemical one. Initially, the material exists as a sheet of metal germanium sulfide "wrapped around" the surfactant. During thermal treatment, the surfactant undergoes fragmentation beginning at ca. 200 °C. The loss of surfactant from the pores makes room for the inorganic sheets to buckle and occupy the space that is created. Whereas the silica walls of MCM-41 are able to undergo condensation−polymerization of residual hydroxyls, heal, and reconstruct to thicken and maintain the integrity of the material, the metal germanium sulfide sheets can only fold. This is illustrated in Scheme 1. There are two consequences of this "crumpling" mechanism that are expected from PXRD: the $d_{100}$ peak will shift to lower values, and the $d_{100}$ peak will broaden (the crystallinity of the material will seem to be lost). These were both observed during the high-temperature PXRD experiment. Yet, the overall order of the material could be maintained, and it is conceivable that the mesostructure could be "re-inflated" in an appropriate medium with added surfactant. It may also be possible to chemically reinforce the walls, thereby stabilizing the mesostructure to collapse on removal of the surfactant template.

**Scheme 1**

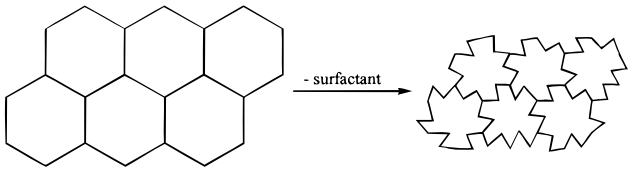


## Conclusions

We have discovered a new class of non-oxide mesostructured materials with hexagonal symmetry. The supramolecular assembly of adamantanoid $[Ge_4S_{10}]^{4-}$ clusters in the presence of transition metals is a new synthetic strategy for developing metal sulfide-based materials with mesostructural and hierarchical order. It should be possible to extend this paradigm to other transition metals and clusters to form an assortment of interesting materials.

The supramolecular organization of the materials is very similar to that of mesoporous silica (MCM-41), whereas the molecular structure is analogous to that of microcrystalline $TMA_2MGe_4S_{10}$ frameworks. Indeed, transition metals are linked to the $[Ge_4S_{10}]^{4-}$ clusters in the final material. In the cases of M = $Zn^{2+}$ and $Co^{2+}$, the *meso*-M/$Ge_4S_{10}$ materials contain tetrahedral metal sites coordinated to the $[Ge_4S_{10}]^{4-}$ clusters. When M = $Ni^{2+}$, however, evidence suggests that the metal is in either a distorted octahedral or square-planar geometry but not tetrahedral. In the case of M = $Cu^+$, our data supports the presence of Cu(I)−Cu(I) dimers in the material.

Mesostructured CTA−Cu/$Ge_4S_{10}$ is thermally stable to 200 °C and retains a high degree of order to nearly 400 °C. A thermal transformation, where the framework undergoes a physical collapse rather than a chemical decomposition, was proposed. This collapse may be circumvented by thickening and strengthening the walls with extra $M^{n+}/S^{2-}$ ions, or by choosing stronger $M^{3+}$ cations to link the clusters.

There are many further investigations of these materials that could be pursued. Their electronic properties, adsorption properties, and chemistry in the channels would be fascinating. Materials of this genre may be useful for cleaning up heavy metal spills and for use in chemical sensors.

**Acknowledgment.** We are grateful to the Natural Sciences and Engineering Research Council (NSERC) and UOP for funding this research. We thank Emmanuel Chomski for technical assistance with Figure 12 and Simon Bare (UOP) for collecting and analyzing the EXAFS data. M.J.M. thanks NSERC for a postgraduate scholarship (1995−99). G.A.O. acknowledges the Canada Council for the award of an Isaac Walton Killam research fellowship (1995−97).

JA992663Q